Vol. 24, No. 1(2025) Sim24364
Revista Mexicana de Ingeniería Química

Arsenate modulation of CYP2C8 heteroenzime electronic properties: An evaluation from density functional theory

Modulación de las propiedades electrónicas de la heteroenzima CYP2C8 por arseniato: Una estimación por teoría del funcional de la densidad

P.G. Nieto-Delgado[1,2], J.G. Rodríguez-Zavala[3], A.A. Vértiz-Hernández[3], J.D. Sánchez-Vásquez[1]*
[1]Departamento de Físico-Matemáticas, Universidad Autónoma de San Luis Potosí (UASLP) San Luis Potosí, SLP, México.
[2]Departamento de Ciencias Exactas y Tecnología, Centro Universitario de los Lagos, Universidad de Guadalajara (U de G) Lagos de Moreno, Jalisco, México.
[3]Unidad Académica Multidisciplinaria Región Altiplano, Universidad Autónoma de San Luis Potosí (UASLP) Matehuala, SLP, México.
Received: June 28, 2024; Accepted: November 11, 2024

Abstract
This study investigates the structural, electronic, and spin polarization properties of different molecular models of the CYP2C8 enzyme, focusing on the effects of arsenate (AsO_4^{3-}) binding to the heme group. Using density functional theory (DFT) calculations, we explored the interactions between arsenate and the iron (Fe) center of the heme group across three models with varying amino acid compositions. Despite structural variations, the charge density and polarization properties remained consistent across models. In the absence of arsenate, the heme group exhibited a dipolar moment with Fe showing a charge of approximately -0.12e and cysteine 435 sulfur (S) having a charge of 0.28e. Strong positive polarization was observed in Fe (1.77 μB), while S showed a smaller polarization (~0.19 μB). Upon arsenate introduction, AsO_4^{3-} bonded with the Fe center, especially in smaller amino acid models, with the As-Fe bond distance optimized to 3.3–3.4 Å. The presence of arsenate reduced the charge on the sulfur atom to approximately 0.17e, significantly decreasing the Fe-S dipolar moment. Additionally, the Fe polarization slightly decreased (to 1.65–1.67 μB), and the sulfur polarization became almost negligible (~0.01 μB). The oxygen atoms of the arsenate showed negative spin polarization (up to -0.43 μB), altering the system's electronic properties. These results suggest that arsenate binding induces notable changes in the enzyme's electronic environment, potentially affecting its physiological role.
Keywords: Arsenate ions, heme-iron center, CYP2C8 enzyme, drug metabolism, DFT.

Resumen
Este trabajo investiga las propiedades estructurales, electrónicas y de polarización de espín de diferentes modelos moleculares de la enzima CYP2C8, centrándose en los efectos de la unión del arsenato (AsO_4^{3-}) al grupo hemo. Utilizando cálculos de la teoría funcional de la densidad (DFT), exploramos las interacciones entre el arsenato y el centro de hierro (Fe) del grupo hemo en tres modelos con distintas composiciones de aminoácidos. A pesar de las variaciones estructurales, la densidad de carga y las propiedades de polarización se mantuvieron constantes en todos los modelos. En ausencia de arsenato, el grupo hemo exhibió un momento dipolar con Fe mostrando una carga de aproximadamente -0,12e y la cisteína 435 azufre (S) teniendo una carga de 0.28e. Se observó una fuerte polarización positiva en Fe (1.77 μB), mientras que S mostró una polarización menor (~0.19 μB). Tras la introducción del arsenato, el AsO_4^{3-} se unió al centro de Fe, especialmente en modelos de aminoácidos más pequeños, con la distancia de enlace As-Fe optimizada a 3.3–3.4 Å. La presencia de arsenato redujo la carga del átomo de azufre a aproximadamente 0.17e, disminuyendo significativamente el momento dipolar Fe-S. Además, la polarización del Fe disminuyó ligeramente (a 1.65–1.67 μB), y la polarización del azufre se volvió casi insignificante (~0.01 μB). Los átomos de oxígeno del arsenato mostraron una polarización de espín negativa (hasta -0.43 μB), alterando las propiedades electrónicas del sistema. Estos resultados sugieren que la unión del arsenato induce cambios notables en el entorno electrónico de la enzima, lo que potencialmente afecta su función fisiológica.
Palabras clave: Iones arseniato, grupo hemo, enzima CYP2C8, metabolismo de fármacos, DFT.

* *Corresponding author. E-mail*: daniel.vasquez@uaslp.mx;
https://doi.org/10.24275/rmiq/Sim24364
ISSN:1665-2738, *issn-e*: 2395-8472

1 Introduction

Metabolism, a critical pharmacokinetic process in drug characterization, often underlies bioavailability issues, drug-drug interactions, and metabolic idiosyncrasies (Lee *et al*., 2024). Executing this process is Cytochrome P450 (CYP), an enzyme complex superfamily of microsomal hemoproteins with 57 functional genes in humans, grouped into 18 families and 44 subfamilies. CYP 450 is expressed in various tissues, including the small intestine and liver, primarily in the endoplasmic reticulum, where genetic regulators bind to chemical inducers, hormones, growth factors, cytokines, and nuclear receptors (Zhao *et al*., 2021). One-third of CYP isoforms are involved in phase 1 metabolism of endo- and exogenous chemicals like steroids, biliary acids, fatty acids, eicosanoids, xenobiotics, environmental contaminants, and carcinogens. These enzymes, affected by polymorphisms and non-genetic factors like gender, age, disease, hormonal influence, and diurnal variations, play a pivotal role in pharmacogenetics and environmental toxicology. They serve as tools to evaluate interactions with drugs, between drugs and environmental xenobiotics, and interactions of endogenous metabolism (Gilani & Cassagnol, 2020).

CYPs, comprising 420-503 heme-protein amino acids in eukaryotes, utilize a thiol group (-SH) as a fifth ligand to the iron atom (Fe) in the heme group, with a highly conserved cysteine as the sixth ligand. Structural similarity is relatively low, with the C-terminal more conserved than the N-terminal (Gilani & Cassagnol, 2020). Anchoring to the membrane occurs via a hydrophobic helix near the N-terminal, positioning the majority toward the membrane's cytosolic face, followed by basic amino acids interacting with lipid charges (Gilani & Cassagnol, 2020; Lamb & Waterman, 2013). The Fe atom in CYP 450 enzymes is in a low-energy state, coordinating with four atoms of nitrogen and the cysteine's sulfur atom. Binding confers absorption at 450 nm when the ferrous form binds to carbon monoxide, and interactions with xenobiotics, especially drugs, occur at the Fe atom (Z. Li *et al*., 2020).

CYP 450 demonstrates vast functional versatility, catalyzing oxidation reactions (aromatic hydroxylation, aliphatic oxidation, desulfurization, N- and S-oxidations, epoxidations, O-, N-, and S-dealkylations, deamination, desulfurization, dehalogenations, and dehydrogenations), reduction, hydrolysis, and hydration. Key players in drug metabolism reactions are the liver isoenzymes CYP 3A4 and CYP 2C8, constituting 52% of the metabolized drugs (Zhao *et al*., 2021).

Certain toxic substances, like heavy metals, interact significantly with CYP. For instance, Naraharisetti and colleagues in 2008 (Naraharisetti *et al*., 2008), using a mouse model, found that 40-ppb arsenic concentrations in drinking water negatively regulate various CYP enzymes, including CYP1A1/2, CYP 2B, CYP 3A4, and CYP 3A23. In 2009, Medina-Diaz and colleagues (Medina-Díaz *et al*., 2009) observed that a 5-mg/kg dose of sodium arsenite over 28 days reduces P450 cytochrome activity by inducing heme oxygenase 1. Noreault and coworkers in 2005 (Noreault *et al*., 2005; Liu *et al*., 2024), using a rat model, determined that 2.5-5 micromolar arsenic concentrations can bind to nuclear receptors involved in CYP 3A4 and CYP 2C8 expression, decreasing their ability to bind ligands and transcription factors. A mouse model study from Xie *et al*. (2007) showed that genes encoding CYP 450 enzymes decrease when exposed to an 84-ppb arsenic concentration in drinking water.

Arsenic (As), a widely distributed environmental metalloid, naturally occurs in the Earth's crust at 5 mg/kg abundance (Guo *et al*., 2024). Forming sulfur-containing mineral compounds, it coexists with silver (Ag), lead (Pb), copper (Cu), nickel (Ni), antimony (Sb), iron (Fe), and cobalt (Co) (Henke, 2009). Resulting from volcanic or mining activities, underground water may exceed 100 μg/L concentrations (Henke, 2009). In surface waters, concentrations are typically <10 μg/L, but anthropogenic sites can surpass 5 μg/L (Mandal *et al*., 1996). The permissible limit in drinking water is 10 μg/L (World Health Organization, 2022), yet certain regions, including West Bengal, Bangladesh, Taiwan, Northern China, Hungary, Mexico, Chile, Argentina, parts of the USA, Thailand, Ghana, Greece, and Austria, may reach up to 50 μg/L (Henke, 2009). Techniques such as functionalized polypropylene membranes and electrocoagulation treatments have shown promise for arsenic removal from contaminated water sources, demonstrating the need for accessible and effective removal solutions to meet regulatory standards (Molina-Jacinto, 2024; Bastida-Vázquez, 2024; Díaz-González, 2023).

Arsenic exists in oxidation states of +3 and +5, forming oxyanions of arsenite (H_3AsO_3 or H_2AsO^{3-} at pH ~9-11) and arsenate (H_2AsO^{4-} and $HAsO_4^{2-}$ at pH ~4-10). Biotransformation in the human body involves converting As^{+5} to As^{+3} and successive methylations, resulting in mono- and dimethylated forms in the liver at a pH range of 7 to 7.4 (Ahmed Baig *et al*., 2010; El-Ghiaty *et al*., 2024). This process poses health risks and affects drug and toxin metabolism (Shen *et al*., 2013). The complexity of arsenic contamination across varied geographic locations also highlights the need for comprehensive water quality assessment and categorization frameworks that can identify and

mitigate risks effectively (Díaz-González, 2023; Liu *et al*., 2024).

Recently, results in the literature provide examples of in-silico methods (Ford *et al*., 2015), which comprise a constantly evolving field useful for studying drug metabolism or drug design. Among several analyses, docking studies are particularly useful, as they allow for evaluation of protein interactions with various substrates (Mishra, 2011). Other computational models are employed to observe toxicity interactions (C. Lewis & O. Miners, 2013; Terrones-Gurrola *et al*., 2023) and protein regulation (Sgrignani *et al*., 2014). Additionally, molecular dynamics simulations have led to novel strategies for specific drug design (J. Li *et al*., 2014). Here, Density Functional Theory (DFT) emerges as a strong theoretical alternative for studying such systems due to its ability to model charge fluctuations. Specifically, DFT modeling has been performed on CYP3A4, demonstrating the binding ability of arsenic ions to the heme group of CYP, though questions remain regarding potential changes in electron density, magnetic polarization, and structural alterations with an expanded model that includes additional amino acids.

In this study, we propose three restricted molecular models of the CYP2C8 heteroenzyme for DFT calculations on the Cytochrome P450 (CYP 450) protein heme group and its surrounding amino acids, including the Fe nucleus. The aim is to quantify local effects—both structural and in terms of charge density and spin polarization—caused by the presence of the Arsenate ion (AsO_4^{3-}) near the Fe nuclei.

2 Methods

- In-silico Analysis of Interaction of Isoenzyme CYP 2C8 with As. The sequences of both enzymes were obtained from the NCBI nucleotide database (Dmitriev, 2021). CYP 2C8 has 39,726 base pairs in its specific gene sequence, for the crystallographic structures of the sequences, we used the PyMOL software (Molecular Graphics System, Version 1.7 Schrödinger, LLC) installed on an core i5 desktop computer.

- The density functional theory (DFT) analysis of the isoforms was based on an in-silico study using a mathematical algorithm on a five-core computer for fast convergence, determining the structure with the lowest energy. The DFT approach was employed to obtain the structural, electron properties, and spin polarization of our molecular models concerning a heme group and the surrounding amino acids. For the electron-ion interaction, we utilized the ultra-soft pseudopotential approximation and a plane wave basis set, implemented in the PWscf code (Giannozzi *et al*., 2009). To optimize computational resources, we selected parameters based on the size of the molecular model.

- For the first and second models, an energy cut-off for plane wave expansion of 512 eV was chosen, while the third model utilized 608 eV. In the case of a cubic supercell, a 32-Å side dimension was employed for the first and second models, and 38-Å for the third model. Brillouin-zone integration was conducted using the ? point. The Perdew-Wang (PW91) gradient-corrected functional (Perdew & Yue, 1986) was employed, and constrained structural optimizations were performed using the Davidson diagonalization method (Davidson, 1975). Convergence in energy was set at 1 meV, and structural optimization continued until forces on each atom reached values of <1 meV/Å. Löwdin population analysis was used to obtain electronic occupations for all atoms in our molecular structure.

3 Results and discussion

3.1 Setting the molecular models

To generate the molecular models, we begin with the crystallographic data of the highest resolution available for CYP2C8 in the PDB (1PQ2) (Schoch *et al*., 2004). Figure 1a depicts the structure of CYP2C8. To streamline the system for DFT methodology, optimizing resources and computing time, we simplify by sequentially adding amino acids closest to the Fe nucleus within average radial distances of 4 Å, 5 Å, and 6 Å. This results in molecular models containing 89, 101, and 163 atoms, respectively.

A crucial component present in all molecular models is the heme group, and we introduce proposed changes around its structure. First, Cysteine 435 (C435) is added. The structural optimization yields a working model referred to as "model 1" (Figure 1b). In Figure 1c, we present the same as in model 1, along with Alanine 297 (A297). These two amino acids, along with the heme group, constitute "model 2." "Model 3" includes the atoms in model 2, along with Glycine 298 (G298), Threonine 301 (T301), Alanine 436, Glycine 437, and Phenylalanine 438 (F428) (see Figure 1d). Hydrogen atoms corresponding to each model's structure are added for completeness. In all figures, the bonds of hydrogen atoms are depicted as thinner for better visualization of the entire structure.

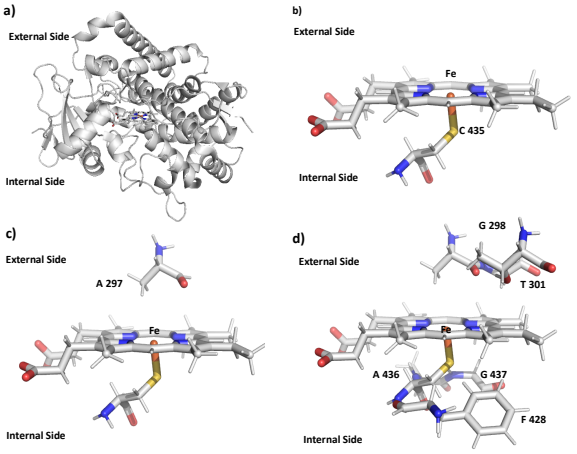

Figure 1. Schematic illustration of the CYP2C8 isoenzyme, highlighting the localization of the iron enzymatic center (a), along with the chemical structures of the iron nucleus models developed in this study: b) Model 1, which includes the heme group, Fe nucleus, and the Cysteine 435 amino acid (C435); c) Model 2, incorporating all elements of Model 1 with the addition of Alanine 297 (A297); d) Model 3, further expanding on Model 2 by including Glycine 298 (G298), Threonine 301 (T301), Alanine 436 (A436), Glycine 437 (G437), and Phenylalanine 438 (F438).

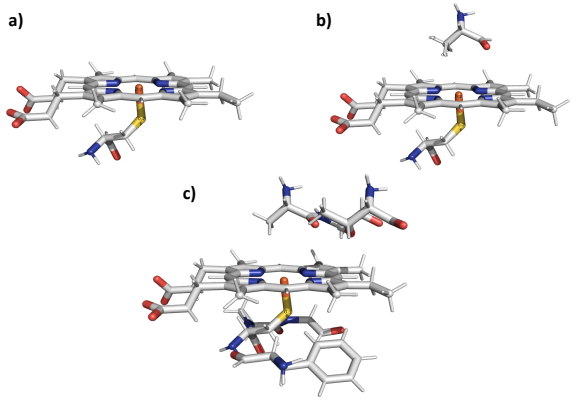

Figure 2. Optimized 3D chemical structures of the proposed models, showcasing the progressive complexity of each model: a) Model 1; b) Model 2; c) Model 3. During the optimization process, only the side chains of the amino acids and the iron atom were permitted to move, illustrating the stability of the core structure in each model.

3.2 *Molecular models analysis*

3.2.1 *Structural changes*

For the structures shown in Figure 1, constrained optimization was performed, considering the movement of the residual part in each amino acid and Fe, while the remaining section of the models was fixed. Figure 2 displays the initial and optimized configurations simultaneously for the three proposed models. In models 1 and 2 (Figures 2a and 2b), slight movements are observed for Fe (0.2 Å) and for the sulfur (0.2 Å) associated with Cysteine 435 when comparing the optimized structure with the initial structures. Additionally, in model 2, there is a displacement in the residual chain CH_3 associated with A297, where the C and two H atoms change their position by 0.1 Å, and the more external H moves by 0.2 Å. On the other hand, in model 3 (Figure 2c), there is only a displacement of 0.1 Å for the sulfur associated with Cysteine 435. Thus, the main structural changes occur in some H atoms in the structure, and no significant structural changes are observed in atoms belonging to the crystallographic data. Particularly, model 3 appears to be the more stable structure, as almost no changes occur when compared to the crystallographic data. The optimized structures in Figure 2 will be referred to as the control structures, upon which later modifications will be made.

3.2.2 *Analysis of charge density and spin polarization*

Figure 3 displays, through a color scale, the charge density (left side) and the magnetic (spin) polarization (right side) of the structures optimized in Figure 2; model 1 in 3a), model 2 in 3b), and model 3 in 3c). The charge density is presented on a scale from -1 *e* to 1 *e*, with red indicating negative charges, blue indicating positive charges, and black indicating neutral charge. In all three models, a greater amount of charge, either positive or negative, is observed in the regions around the heme group. Additionally, there is an almost neutral charge density in the core area of Fe and its closer neighbors. Notably, there is a charge of -0.12, -0.12, and -0.14 *e* for Fe and a charge of 0.28, 0.28, and 0.25 *e* for the S of C435 in models 1, 2, and 3, respectively. Both atoms contribute to a dipole moment in the structure of the heme group.

Furthermore, in model 2, there is a negative charge on the residual chain carbon of A297 (-0.46 *e*). However, when considering the electrical charge of the three associated hydrogen atoms and the complete residual chain of Alanine, a charge of 0.13 *e* is observed for the carbon of the residual chain of the same residue A297. In the case of model 3, a negative electrical load of -0.46 *e* is observed for the carbon, and the total load for the entire chain is 0.12 *e*.

In model 3, the moiety T301 has a lateral chain that can be separated into two main groups: CH_3 and OH. The most negative charges are found in the C of the CH_3 group (-0.49 *e*) and in the O of the OH group (-0.54 *e*). On the other hand, the highest positive charge is in the H of the OH group (0.39 *e*), indicating that this group exhibits a dipolar moment. In summary, for the CH_3 group, there is a charge of 0.12 *e*, neutralizing the negative charge of C when considering the charge

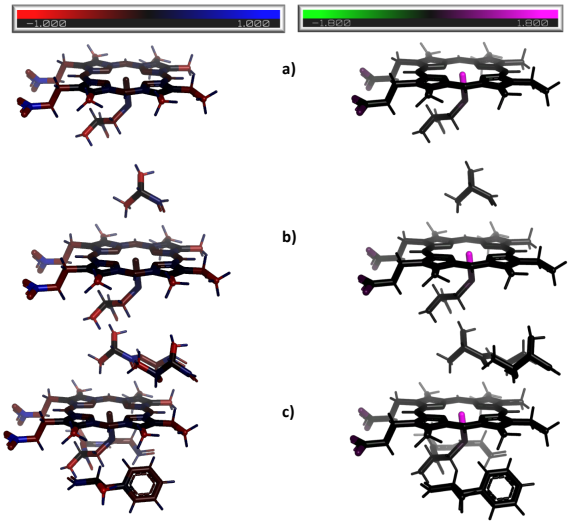

Figure 3. Visualization of effective charge density (left) and magnetic polarization (right) represented with a color gradient for the proposed models: a) Model 1; b) Model 2; c) Model 3. Charge density was calculated using Löwdin's method. The color bar indicates the units: electrons (e) for charge density and Bohr magnetons (μB) for magnetic polarization, both measured per cell.

of the hydrogens associated with the CH_3 group. A similar situation occurs with the OH group, with a total charge of -0.14 *e*. For the entire lateral chain of T301, the charge is 0.27 *e*.

In short, for the three models, similar charges are observed around the heme group and in common moieties. Although some atoms show significant charges, the complete chains exhibit a certain neutralization or shielding effect of the charge.

Regarding polarization, as shown on the right side of Figure 3, a color scale ranging from -1.8 μB to 1.8 μB is used, where green represents negative polarization, pink indicates positive, and black signifies the absence of polarization. In the three models, almost identical distributions are observed, all displaying a strong positive polarization in the Fe nucleus, with polarizations of 1.76, 1.77, and 1.79 μB obtained for models 1, 2, and 3, respectively. Figure 3 also illustrates polarization in the four oxygen atoms of the heme group, averaging 0.4 μB. A relatively small polarization is noted in the S of C435, with values of 0.19, 0.19, and 0.16 μB for models 1, 2, and 3 respectively. It should be mentioned that none of the amino acids added in model 2 or 3, compared to model 1, presented any polarization.

Equivalent to the optimization of each proposed molecular model (Figure 2), both in charge density and polarization, the three models exhibit very similar distributions despite having different numbers of amino acids. Therefore, it can be considered that increasing the number of amino acids in our models will not produce significant changes in the obtained results. In the next section, we will analyze how the structure, charge density, and spin polarization will be affected by the presence of Arsenate.

3.3 Effects on arsenate on molecular models

3.3.1 Structural changes

The effects of the arsenate ion (AsO_4^{3-}) on the proposed molecular models were quantified in the control structures. First, the structure of arsenate was optimized with a total charge of -3 *e* for the ionic complex, resulting in a pyramidal molecular arrangement with a triangular base and arsenic (As) in the center. The distance between As and any of the oxygen atoms was 1.7 Å.

After optimizing the AsO_4^{3-} structure, the ion was placed over the iron center in all the control structures to simulate a possible interaction of arsenate with the enzyme from the extracellular side. For the input structures, the AsO_4^{3-} was positioned at three different As-Fe distances: 4 Å, 5 Å, and 6 Å, over the line that forms the sulfur atom of C435 and the Fe.

In addition to the initial distance variation, three initial orientations for the AsO_4^{3-} ion were proposed: 1) Random, where the optimized pyramidal AsO_4^{3-} does not have a preferential orientation toward the Fe center of the model structures (Figure 4a), 2) Base position, where one triangular face of the AsO_4^{3-} is oriented toward the Fe center (Figure 4b), and 3) Inverted pyramid, where one of the vertices of the AsO_4^{3-} is oriented toward the Fe center (Figure 4c). In total, nine initial configurations were constrained and optimized, allowing structural changes of the amino acid moieties, and the arsenate ion and the iron center were allowed to move in every model. In all cases, the optimization of charge density has no restrictions.

Figure 4d displays the most stable configuration obtained from the optimized initial configuration with a pyramidal base orientation and 4 Å of As-Fe distance. After optimization, the distance between the As and Fe atoms is 3.3 Å, and the distance between the O and Fe atoms is 1.8 Å. The AsO_4^{3-} ion structure undergoes slight changes, with the distance between the As and the O atom bonded to the Fe center changing to 1.8 Å, while the other O atoms remain at 1.7 Å from the As center atom. It is noteworthy that, for every initial configuration with model 1—shown in Figure 4a, b, and c, similar results are obtained, with the AsO_4^{3-} bonded to the Fe center. However, the distance between the As and the Fe center is 3.4 Å for Figure 4b.

The same initial configurations depicted in Figure 4 (a-c) were optimized with the model 2 structure. In this case, the most stable configuration (Figure 5a) resulted from the initial inverted pyramid orientation and a 5 Å As-Fe distance. Additionally, the Fe is now

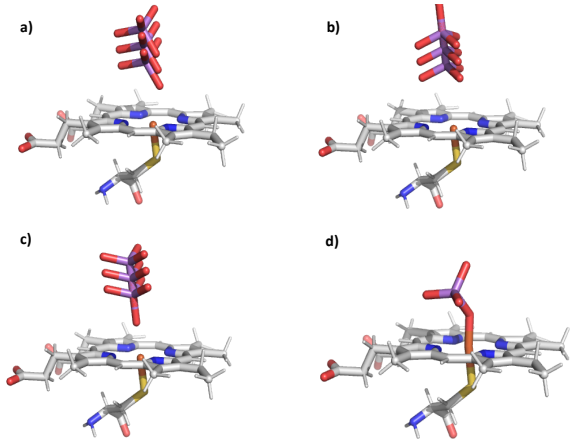

Figure 4. Three-dimensional schematic representation of the initial arsenate positioning scenarios explored for Model 1: a) Initial configuration 1; b) Initial configuration 2; c) Initial configuration 3; and d) Optimized structure showing the lowest energy configuration derived from all initial setups.

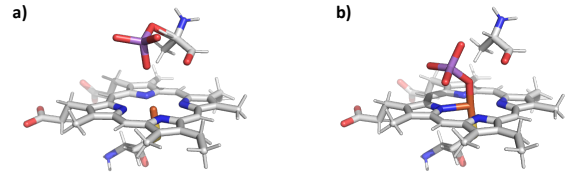

Figure 5. Three-dimensional schematic representation of Model 2 interacting with arsenate, focusing on the scenario that produced the lowest energy structure: a) Initial position of arsenate; b) Optimized configuration after interaction.

bonded with one of the N atoms of the heme group, decreasing the distance between the Fe and the N from 2.1 Å to 2 Å. When an initial pyramidal base orientation was optimized, in some cases, the cleavage of atomic bonds in the present amino acid occurred due to the strong repulsion between the O atoms from the AsO_4^{3-} and the nearby A297; these structures were dismissed from the stability analysis.

During the optimization process for initial configurations with As-Fe distances of 4 and 5 Å, and both pyramidal base and inverted pyramid orientations, the AsO_4^{3-} spontaneously bonded to the Fe center. However, in cases with an initial As-Fe distance of 6 Å, the AsO_4^{3-} remained near its initial position. All optimized structures for model 1 showed the AsO_4^{3-} bonded to the Fe center. In contrast, not all optimizations for model 2 exhibited this bond. Nonetheless, the most stable structures in model 2 were those with a bond between the AsO_4^{3-} and the Fe center.

The configuration shown in Figure 5b is similar to the one in Figure 4d. The distance between the O and Fe atoms is 1.8 Å, and the distance between the As and the O atom bonded to the Fe center is 1.8 Å, while the other O atoms remained at 1.7 Å from the As center

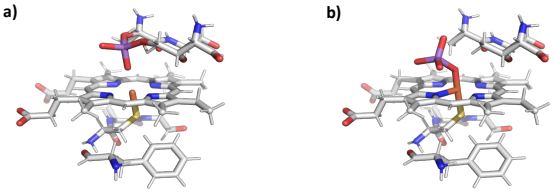

Figure 6. Three-dimensional schematic representation of Model 3 interacting with arsenate, highlighting the scenario that yielded the lowest energy structure: a) Initial position of arsenate; b) Optimized configuration following the interaction.

atom. However, the distance between the As and the Fe center is 3.4 Å for Figure 5b.

The same process of proposing nine initial configurations has been conducted with the model 3 structure. Figure 6a shows the initial configuration, which, after optimization, yields the most stable configuration shown in Figure 6b. The inverted pyramid orientation and the As-Fe distance of 4 Å were the initial configurations that gave the most stable structure. Like Figure 5b, the Fe atom is bonded with one of the N atoms of the heme group, and the Fe-N distance is also decreased from 2.1 Å to 2 Å.

In the case of optimized structures for model 3, the bond between the Fe atom from the heme group and the AsO_4^{3-} ion was only observed with a 4 Å As-Fe distance, under both random and inverted pyramid orientations for initial configurations. The final position of the AsO_4^{3-} is very similar to the one observed in Figure 5b, except for the distances of As-Fe; in Figure 6b, they change to 3.4 Å and 1.8 Å, respectively. The distance between the As and the O atom bonded to the Fe center changed to 1.9 Å, while the other O atoms remained at 1.7 Å from the As center atom.

In brief, the AsO_4^{3-} bonded with the Fe center is more likely to be observed in structures with fewer amino acids. When more amino acids are attached to each of the model structures, the chances of having the AsO_4^{3-} bonded to the Fe decrease. In all cases, the most stable structures are the ones that present the AsO_4^{3-} ion bonded to the Fe center.

3.3.2 Charge density and spin polarization in presence of arsenate

Charge density and spin polarization were calculated for each optimized structure to observe the effect of the AsO_4^{3-} ion on electronic properties. Figure 7 presents the charge density of the most stable structures for the three models on the left side, while on the right, the polarization of the same structures is shown. The scales and colors are consistent with those in Figure 3. The most stable structure of model 1 is shown in Figure 7a, while the most stable structures of models 2 and 3 are depicted in Figures 7b and 7c, respectively.

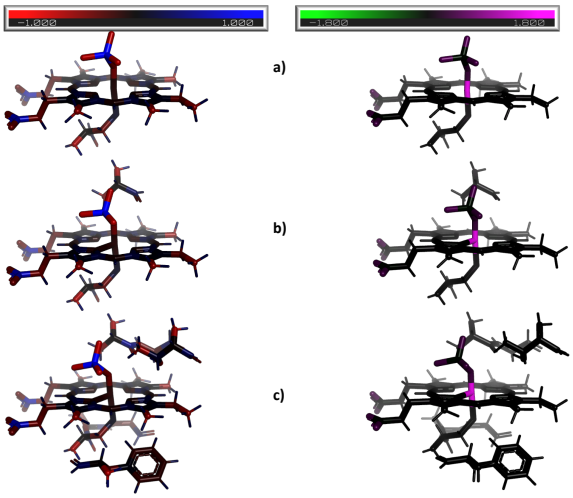

Figure 7. Effective charge density (left side) and magnetic polarization (right side) depicted with a color gradient for the proposed models including arsenate: a) Model 1; b) Model 2; c) Model 3. Charge density was calculated using Löwdin's method. The color bar units represent "electrons" for charge density and "Bohr magnetons" for spin polarization.

Regarding the charge density, the results are remarkably similar to those seen in the model structures in the absence of the AsO_4^{3-} ion. A high charge density is observed in the region surrounding the heme center, with a neutral charge close to neutral near the Fe center and its neighboring atoms. For each structure in Figure 7, charges of -0.11, -0.13, and -0.14 *e* are observed for the Fe atom, and 0.17, 0.17, and 0.12 *e* for the S atom in C435. The charge density obtained for the Fe in each structure is alike to the one calculated in the absence of the AsO_4^{3-}. However, there is a change in the charge density of the S atom in C435, about 40% less than that calculated for the model structures, thus altering the Fe-S dipolar moment.

Similarly, as in Figure 3, Figure 7 shows an important charge distribution in the amino acids attached in models 2 and 3, although the values of the charge density remained almost the same. The A297 moiety in Figure 7b has a charge of 0.14 *e*, and for the A297 and T301 moieties in Figure 7c, charge values of 0.14 and 0.31 *e* were observed. Hence, for the three stable structures with the AsO_4^{3-} ion present, as seen in Figure 7, we observed comparable charge values for the heme group and the attached amino acids, with the exception of the S atom in C435.

The charges calculated for the As atom in the three models are 1.87, 1.86, and 1.84 *e*, and the calculated charges of the O atom that is bonded with the Fe center are -0.43, -0.42, and -0.41 *e*. The rest of the O atoms in the arsenate that are not bonded have an average charge of -0.62, -0.64, and -0.66 *e*. The total charge of the AsO_4^{3-} ion in the three cases was -0.42, -0.48, and -0.54 *e*. Being a structure with such charge density, as is the AsO_4^{3-} ion, it is evident why this ion can change the CYP2C8 immediate environment.

In terms of polarization, as shown in Figure 7, the three proposed models exhibit almost identical polarization distributions. Similar to Figure 3, a strong positive polarization of the Fe can be observed, with values of 1.67, 1.67, and 1.65 μB for each model. In all cases, the calculated polarization was less than that calculated for the model structures. There is also a noticeable polarization of the oxygen atoms of the heme group, with a calculated average of 0.41 μB for those atoms.

The average polarization calculated for the structures presented in Figure 7 was 0.05, 0.03, and -0.01 μB for each model. It should be observed that the polarization of the S atom in C435 is almost imperceptible, and it can be affirmed that the polarization of that S atom disappears in comparison with the polarization calculated for the same atom in the control model structures.

There is also a change in polarization in the oxygen atoms of the AsO_4^{3-} once they are bonded with the Fe center. Those atoms have an average polarization of 0.47, 0.43, and 0.39 μB for each model, with the smallest polarization in the O atom bonded to the Fe. Thus, we have demonstrated that the presence of the AsO_4^{3-} ion changes the polarization of the CYP2C8.

As in the electrical charge analysis, the results seem similar among the structures presented in Figure 7. The Fe center's polarization decreases in all three models, and the S atom in C435 loses almost all polarization. On the other hand, the main change in spin polarization in all structures, compared to control ones, occurs due to the presence of AsO_4^{3-}, as the associated oxygen atoms present a negative spin polarization in all of them.

In-silico information from DFT modeling supports that the charge density for the heme group (Fe^{++2}) of CYP 2C8 does not allow charge transfer in the presence of As (AsO_4^{3-}) by virtue of its high electronegativity, As modifies the charge of the environment with the consequent displacement of Fe^{++2} which modifies the metabolic action of the isoform (El-Ghiaty *et al.*, 2024). Many authors, such as Naraharisseti and his group document the fact that As decreases the expression of proteins including those of cytochrome P450 (Naraharisetti *et al.*, 2008). Also, there is evidence that As [> 0.005 ppm As in urine], dimethyl arsenic (DMA) and monomethyl arsenic (MMA) in cell nucleus receptors bind and consequently decrease cytochrome P450 isoform expression and metabolic action (Noreault, 2005).

Alterations due to As in protein groups of metabolic importance in load and functionality of the heme group (isoforms of cytochrome P450) are

associated with pathologies such as some types of cancer, hyperkeratosis, alterations in the metabolism of drugs and xenobiotics, diabetes mellitus, among others, therefore, the study of As on proteins is of utmost importance.

The spin polarization results obtained in this study align with previous findings on metalloproteins and transition metal complexes. For instance, studies on copper complexes mimicking superoxide dismutase activity demonstrated how metal-ligand interactions can influence electronic properties, with spin polarization and charge transfer being key factors in their biological activity (Silva *et al*., 2023). Similarly, investigations on zinc-binding metalloproteins using DFT calculations have provided insights into how the spatial arrangement of metal ions within enzyme active sites affects their electronic structure, influencing both charge density and polarization (Barbosa et al., 2021). These studies offer a solid context for understanding how arsenate binding affects the Fe and S atoms in CYP2C8.

Furthermore, our observations that arsenate induces subtle changes in charge density and polarization are comparable to other metal-protein interactions. DFT studies on lactoferrin, an iron-binding glycoprotein, have shown how metal binding induces charge redistribution in the surrounding ligating residues, impacting the overall electronic structure and function of the protein (Honarparvar *et al*., 2019). These findings are consistent with the changes observed in our models, where the arsenate ion significantly influences the Fe and S atom polarization, akin to the behavior seen in other metal-binding proteins.

Finally, the broader implications of our study resonate with recent advancements in de novo metalloprotein design, which explore how ligand geometry and metal coordination affect protein function. By mimicking natural systems and incorporating novel metals, researchers have demonstrated that precise control over metal-binding properties can be achieved, as seen in our analysis of arsenate's interaction with CYP2C8 (Chalkley *et al*., 2021).

Conclusions

Despite using different simplified models of CYP2C8 in this study, the results for structural properties, charge density, and magnetic polarization were consistent, indicating the reliability of the calculations even with a truncated CYP2C8 protein model.

In the control models without arsenate, a dipolar moment was observed in the heme group, primarily due to the negative charge of the iron (Fe) and the positive charge of sulfur (S) in C435. Additionally, a notable positive polarization in Fe and minor polarization in S was recorded.

In the arsenate-bound models, we demonstrated the feasibility of arsenate binding to the iron center, even though this binding did not occur spontaneously in all initially proposed configurations. The optimal configuration in each model was achieved with arsenate (AsO43-) bonded to the Fe center. While this bonding did not induce drastic changes in the charge density or polarization of the iron center, the sulfur in the C435 moiety lost a significant portion of its positive charge, reducing the dipolar moment of the original structure. This sulfur atom also lost almost all its polarization when arsenate was present.

The arsenate-bound structure exhibited substantial charge density, with a highly positive As atom and negatively charged O atoms, contributing to the positive polarization of the system. These changes in electronic properties suggest that arsenate may alter the physiological function of CYP2C8.

Moving forward, experimental validation of these computational findings, such as binding affinity assays and structural analysis using X-ray crystallography or NMR spectroscopy, would be crucial to confirm the predicted arsenate interactions with CYP2C8. Future research should also explore the thermodynamic and kinetic properties of these interactions under physiological conditions, which would provide a more comprehensive understanding of CYP2C8's role in arsenic metabolism and its broader biological implications.

Acknowledgements

PGND and JGRZ acknowledge to PRODEP grant #103.5/13/8598.

The authors thankfully acknowledge the computer resources, technical expertise and support provided by the Laboratorio Nacional de Supercómputo del Sureste de México.

And also, to J. Renteria-Arriaga for technical support.

References

Baig, J. A., Kazi, T. G., Shah, A. Q., Kandhro, G. A., Afridi, H. I., Arain, M. B., Jamali, M. K, & Jalbani, N. (2010). Speciation and evaluation of Arsenic in surface water and groundwater samples: A multivariate case study. Ecotoxicology and Environmental Safety, 73(5), 914–923. https://doi.org/10.1016/J.ECOENV.2010.01.002

Barbosa, E. D., Lima Neto, J. X., Teixeira, D. G., Bezerra, K. S., do Amaral, V. S.,

Oliveira, J. I. N., Santos Lima, J. P. M., Machado, L. D., & Fulco, U. L. (2021). Exploring human porphobilinogen synthase metalloprotein by quantum biochemistry and evolutionary methods. Metallomics, 13(4), 17. https://doi.org/10.1093/MTOMCS/MFAB017

Bastida-Vázquez, J., Roa-Morales, G., Gómez-Espinosa, R. M., Balderas-Hernández, P., & Natividad-Rangel, R. (2024). Water treatment applying electrocoagulation and filtration processes with a functionalized membrane of a contaminated water body from San Cayetano de Morelos, Toluca. Revista Mexicana de Ingeniería Química, 23(1) IA24164. https://doi.org/10.24275/rmiq/IA24164

Chalkley, M. J., Mann, S. I., & DeGrado, W. F. (2021). De novo metalloprotein design. Nature Reviews Chemistry, 2021 6(1), 31–50. https://doi.org/10.1038/s41570-021-00339-5

Davidson, E. R. (1975). The iterative calculation of a few of the lowest eigenvalues and corresponding eigenvectors of large real-symmetric matrices. Journal of Computational Physics, 17(1), 87–94. https://doi.org/10.1016/0021-9991(75)90065-0

Díaz-González, L., Rosales-Rivera, M., & Chávez-Almazán, L. A. (2023). Comprehensive assessment of groundwater quality in Mexico and application of new water classification scheme based on machine learning. Revista Mexicana de Ingeniería Química, 22(2), IA235. https://doi.org/10.24275/rmiq/IA235

Dmitriev, A. V., Rudik, A. V., Karasev, D. A., Pogodin, P. V., Lagunin, A. A., Filimonov, D.A., & Poroikov, V. V. (2021). In Silico Prediction of Drug-Drug Interactions Mediated by Cytochrome P450 Isoforms. Pharmaceutics, 13(4), 538. https://doi.org/10.3390/pharmaceutics13040538

El-Ghiaty, M. A., Alqahtani, M. A., El-Mahrouk, S. R., Isse, F. A., Alammari, A. H., & El-Kadi, A. O. S. (2024). Alteration of Hepatic Cytochrome P450 Expression and Arachidonic Acid Metabolism by Arsenic Trioxide (ATO) in C57BL/6 Mice. Biological Trace Element Research. https://doi.org/10.1007/s12011-024-04225-1

Ford, K. A., Ryslik, G., Sodhi, J., Halladay, J., Diaz, D., Dambach, D., & Masuda, M. (2015). Computational predictions of the site of metabolism of cytochrome P450 2D6 substrates: comparative analysis, molecular docking, bioactivation and toxicological implications. Drug Metabolism Reviews, 47(3), 291–319. https://doi.org/10.3109/03602532.2015.1047026

Giannozzi, P., Baroni, S., Bonini, N., Calandra, M., Car, R., Cavazzoni, C., Ceresoli, D., Chiarotti, G. L., Cococcioni, M., Dabo, I., Dal Corso, A., De Gironcoli, S., Fabris, S., Fratesi, G., Gebauer, R., Gerstmann, U., Gougoussis, C., Kokalj, A., Lazzeri, M., & Wentzcovitch, R. M. (2009). QUANTUM ESPRESSO: a modular and open-source software project for quantum simulations of materials. Journal of Physics: Condensed Matter, 21(39), 395502. https://doi.org/10.1088/0953-8984/21/39/395502

Gilani, B., & Cassagnol, M. (2020). Biochemistry, Cytochrome P450. StatPearls. http://europepmc.org/books/NBK557698

Guo J., Cao W., Lang G., Sun Q., Nan T., Li X., Ren Y., & Li Z. (2024). Worldwide Distribution, Health Risk, Treatment Technology, and Development Tendency of Geogenic High-Arsenic Groundwater. Water, 16(3), 478. https://doi.org/10.3390/w16030478

Henke, K. R. (2009). Arsenic: environmental chemistry, health threats, and waste treatment. Wiley. https://www.wiley.com/en-mx/Arsenic%3A+Environmental+Chemistry%2C+Health+Threats+and+Waste+Treatment-p-9780470741139

Honarparvar, B., Kanchi, S., & Bisetty, K. (2019). Theoretical insights into the competitive metal bioaffinity of lactoferrin as a metal ion carrier: a DFT study. New Journal of Chemistry, 43(41), 16374–16384. https://doi.org/10.1039/C9NJ03786A

Lamb, D. C. & Waterman, M. R. (2013). Unusual properties of the cytochrome P450 superfamily. Philosophical Transactions of the Royal Society B: Biological Sciences. 368(1612), 20120434. http://doi.org/10.1098/rstb.2012.0434

Lee J., Beers, J. L, Geffert R. M., & Jackson K. D. (2024). A Review of CYP-Mediated Drug Interactions: Mechanisms and In Vitro Drug-Drug Interaction Assessment. Biomolecules, 14(1): 99. https://doi.org/10.3390/biom14010099

Lewis, B. C., & Miners, J. O. (2013). Generation, Validation, and Application of a P450 Homology Model. Current Models in Medicinal

Chemistry, 13(8), 2233–2240. https://doi.org/10.2174/15680266113136660156

Li, J., Wei, D. Q., Wang, J.-F., Yu, Z. T., & Chou, K. C. (2014). Molecular Dynamics Simulations of CYP2E1. Medicinal Chemistry, 8(2), 208–221. https://doi.org/10.2174/157340612800493692

Li, Z., Jiang, Y., Guengerich, X. F. P., Ma, L., Li, S., & Zhang, W. (2020). Engineering cytochrome P450 enzyme systems for biomedical and biotechnological applications. Journal of Biological Chemistry, 295(3), 833–849. https://doi.org/10.1016/S0021-9258(17)49939-X

Liu Q., Li P., Ma J., Zhang J., Li W., Liu Y, Liu L., Liang S., & He M. (2024). Arsenic exposure at environmentally relevant levels induced metabolic toxicity in development mice: Mechanistic insights from integrated transcriptome and metabolome. Environment International, 190, 108819. https://doi.org/10.1016/j.envint.2024.108819

Mandal, B. K., Chowdhury, T. R., Samanta, G., Basu, G. K., Chowdhury, P. P., Chanda, C. R., Lodh, D., Karan, N. K., Dhar, R. K., Tamili, D. K., Das, D., Saha, K. C., & Chakraborti, D. (1996). Arsenic in groundwater in seven districts of West Bengal, India – The biggest arsenic calamity in the world. Current Science, 70(11), 976–986. http://www.jstor.org/stable/24111635

Medina-Díaz, I. M., Estrada-Muñiz, E., Reyes-Hernández, O. D., Ramírez, P., Vega, L., & Elizondo, G. (2009). Arsenite and its metabolites, MMAIII and DMAIII, modify CYP3A4, PXR and RXR alpha expression in the small intestine of CYP3A4 transgenic mice. Toxicology and Applied Pharmacology, 239(2), 162–168. https://doi.org/10.1016/J.TAAP.2008.11.009

Mishra, N. K. (2011). Computational modeling of P450s for toxicity prediction. Expert Opinion on Drug Metabolism & Toxicology, 7(10), 1211–1231. https://doi.org/10.1517/17425255.2011.611501

Molina-Jacinto, M., Gómez-Espinosa, R.M., & Arizmendi-Cotero, D. (2024). Easy and fast functionalization of polypropylene and its efficiency in arsenic (V) removal. Revista Mexicana de Ingeniería Química, 23(3) IA24334. https://doi.org/10.24275/rmiq/IA24334

Naraharisetti, S. B., Aggarwal, M., Sarkar, S. N., & Malik, J. K. (2008). Concurrent subacute exposure to arsenic through drinking water and malathion via diet in male rats: Effects on hepatic drug-metabolizing enzymes. Archives of Toxicology, 82(8), 543–551. https://doi.org/10.1007/s00204-008-0318-6

Noreault, T. L., Kostrubsky, V. E., Wood, S. G., Nichols, R. C., Strom, S. C., Trask, H. W., Wrighton, S. A., Evans, R. M., Jacobs, J. M., Sinclair, P. R., & Sinclair, J. F. (2005). Arsenite decreases cyp3a4 and rxr? in primary human hepatocytes. Drug Metabolism and Disposition, 33(7), 993–1003. https://doi.org/10.1124/DMD.105.003954

Perdew, J. P., & Yue, W. (1986). Accurate and simple density functional for the electronic exchange energy: Generalized gradient approximation. Physical Review B, 33(12), 8800. https://doi.org/10.1103/PhysRevB.33.8800

Schoch, G. A., Yano, J. K., Wester, M. R., Griffin, K. J., Stout, C. D., & Johnson, E. F. (2004). Structure of Human Microsomal Cytochrome P450 2C8. Journal of Biological Chemistry, 279(10), 9497–9503. https://doi.org/10.1074/jbc.m312516200

Sgrignani, J., Bon, M., Colombo, G., & Magistrato, A. (2014). Computational approaches elucidate the allosteric mechanism of human aromatase inhibition: A novel possible route to small-molecule regulation of cyp450s activities? Journal of Chemical Information and Modeling, 54(10), 2856–2868. https://doi.org/10.1021/ci500425y

Shen, S., Li, X. F., Cullen, W. R., Weinfeld, M., & Le, X. C. (2013). Arsenic binding to proteins. Chemical Reviews, 113(10), 7769–7792. https://doi.org/10.1021/CR300015C

Silva, T. U., da Silva, E. T., Albuquerque, M. G., Lima, C. H. da S., & Machado, S. de P. (2023). DFT calculations of copper complexes mimicking superoxide dismutase and docking studies and molecular dynamics of the transition metal complex binding to serum albumin. Journal of Biomolecular Structure and Dynamics, 42(20). https://doi.org/10.1080/07391102.2023.2259479

Terrones-Gurrola, M. C. del R., Ponce-Peña, P., Salas-Pacheco, J. M., Camacho-Luis, A., Pozos-Guillén, A. de J., Nieto-Delgado, G., López-Guzmán, O. D., & Vértiz-Hernández, A. A. (2023). Arsenic: A Perspective on Its Effect on Pioglitazone Bioavailability. International

Journal of Environmental Research and Public Health, 20(3), 1901. https://doi.org/10.3390/IJERPH20031901

World Health Organization (2022). Guidelines for drinking-water quality: fourth edition incorporating the first and second addenda. https://www.who.int/publications/i/item/9789240045064

Xie, Y., Liu, J., Benbrahim-Tallaa, L., Ward, J. M., Logsdon, D., Diwan, B. A., & Waalkes, M. P. (2007). Aberrant DNA methylation and gene expression in livers of newborn mice transplacentally exposed to a hepatocarcinogenic dose of inorganic arsenic. Toxicology, 236(1–2), 7–15. https://doi.org/10.1016/J.TOX.2007.03.021

Zhao, M., Ma, J., Li, M., Zhang, Y., Jiang, B., Zhao, X., Huai, C., Shen, L., Zhang, N., He, L., & Qin, S. (2021). Cytochrome p450 enzymes and drug metabolism in humans. International Journal of Molecular Sciences, 22(23), 12808. https://doi.org/10.3390/IJMS222312808/S1